SOME ACOUSTIC EFFECTS OF INTERNAL MACROSTRUCTURE

by

R.H. Mellen and D.G. Browning
US Naval Underwater Systems Center
New London, Conn.
U.S.A.

ABSTRACT

Some recent experimental developments relating to internal oceanographic-acoustic interactions are reviewed. Besides amplitude and phase fluctuations, a major concern is scattering into shadow regions. Associated oceanographic phenomena may include shear currents, turbulence and internal waves and upwelling. Experimental data show frequency independence of both scatter into shadow zones and leakage from sound channels. Propagation over sea mounts also shows the dominance of oceanographic refraction over diffraction. Preliminary results of an experiment involving a large ocean eddy are discussed.

INTRODUCTION

FIGURE 1

A modest goal of underwater acousticians is to be able to deal with the variety of oceanographic phenomena that contribute to acoustic variability. Johannessen has appropriately called this effort "parameterizing oceanography for the acoustic problem." Figure 1 is a list of oceanographic phenomena suggested by Paul Scully-Power of RANRL whose main interest, incidentally, is in the acoustic properties of eddies. The list is roughly in order of increasing size and ranges in scale from less than 1 m to the dimensions of the body of water involved. The lower limit is perhaps governed by the acoustic wavelengths of interest, i.e., long wavelengths may pass through thin layers with little or no effect due to the layering itself.

Oceanographic phenomena tend to be interrelated, i.e., shear currents cause instabilities that generate internal waves, which in turn break and produce turbulence. Eddies involve all of these to a high degree because of their high rotational speeds. Scale sizes also tend to overlap so that the vertical scales of layers, turbulence and internal waves may be limited only by the thermocline thickness. At the large end of the scale the problem tends to become deterministic, when a few measurements suffice for the acoustic description. Medwin suggests calling the in-between region where both deterministic and stochastic methods are indicated, the "meso-scale."

SHEAR CURRENTS

FIGURE 2

One of the properties of layers that has received but little attention until recently is acoustic refraction by shear currents. Since sound waves are Galilean relativistic, current gradients follow Snell's Law just as the sound speed gradient itself. Figure 2 shows current measurement by Sanford (reference 1) in the Sargasso Sea. Peak currents are of the order of 10 cm/sec and typical gradients 10^{-3}/sec, roughly a factor of 10 smaller than the barocline.

FIGURE 3

Figure 3 shows the nonreciprocity of sound rays teavelling in opposite directions. Nonreciprocity is significant only where the current gradient dominates, i.e., in regions where the temperature and pressure gradients tend to cancel. However, encounters with random current gradients along the propagation path can produce cumulative scattering. In fact, the possibility of scattering in isothermal turbulent water suggests that microcurrent measurements may be significant in determining the acoustic characteristics. In most cases, however, the flow component of scatter is probably small and temperature effects tend to dominate.

TURBULENT LAYERS AND INTERNAL WAVES

FIGURE 4

A most extreme case of scatter from a turbulent boundary was found by Krauss (reference 2) in the Baltic where the bottom water

layer is overlayed by a colder layer of lower salinity. The interface is evidently unstable and gives rise to very short internal waves which are thought to break and produce patches of turbulence. Figure 4 shows the sound speed profile together with a recording of the backscattered signals from a 30-kHz echo sounder at normal incidence. Particularly strong echoes occur near the lower channel boundary. The possibility of a plankton layer has been discounted and the echo is attributed to backscatter from the turbulent interface.

FIGURE 5

Supporting the argument, the spectrum of the temperature fluctuations shown in Fig. 5 exhibits a peak near the local buoyancy frequency as well as evidence of turbulent activity above this frequency. Porter, et al (reference 3) found similar evidence of internal activity above the buoyancy frequency in their phase fluctuation measurements at Bermuda.

FIGURE 6

Figure 6 shows the phase fluctuation spectrum for 400 Hz acoustic signals compared to the spectrum predicted for internal waves which cuts off near 10 cph.

FIGURE 7

Stanford (reference 4) examined the amplitude as well as phase fluctuations of low frequency signals propagating between Bermuda and Eleuthera. The power spectrum of the amplitude fluctuations in Fig. 7 has a rather stable region up to 20 cph for all observation

periods shown. He attributes the variable portion at higher frequencies to turbulence in the surface layer and the variation with season to changing ray paths.

Beckerle, et al (reference 5) also studied the relationship between internal waves and acoustic temporal fluctuations near Bermuda and showed fair correlation with internal wave activity. Weston (reference 6) has done similar work in shallow water in the Bristol channel. Much of the recent work on fluctuations is covered in other sections of this conference.

FIGURE 8

Some of the other acoustical effects of acoustically disturbed layers may be predicted however. The model shown in Fig. 8 represents a thin smooth layer where the sound speed increases by 1.5 m/sec. For grazing angles less than critical, there is total reflection at the interface and a shadow zone below. For a moderate value of scatter the "shadow zone" illumination becomes fairly strong, in this case about 20 dB below the incident level. The illumination of shadow zones by surface scatter is a well known phenomenon but observations of the internal scatter mechanism are quite recent.

FIGURE 9

Figure 9 illustrates schematically signals reflected from a rough boundary, in this case the ocean surface where the specular reflection is reversed in polarity. The specular arrival is followed by a reverberation tail since all of the scatter paths

involve longer travel time. This reverberation following the specular reflection is a useful characteristic for identifying reflections from a rough interface.

FIGURE 10

If the receiver is on the opposite side of a scattering layer in the shadow zone as shown in Fig. 10 the minimum time path is approximately a straight line from S to R. The diffracted signal arrives later and the level of higher frequencies are reduced depending on the position within the shadow zone. These characteristics are useful in identifying scatter through the interface. Diffuse high frequency precursors of this type have been observed in experiments at the Maltese front.

FRONTS

FIGURE 11

Fronts have been described as boundaries between water masses of different temperatures. The boundaries are complicated and dynamic and give rise to acoustic disturbances. Figure 11 shows a superposition of several SSP's taken at the Maltese front (references 7 and 8) over a twelve-hour period. Frontal conditions were apparently locally stable judging by the node near 100 m. The fluctuations are thought to be internal waves.

FIGURE 12

The wave number spectrum of the "random" part of the SSP for the 300 m column is shown in Fig. 12. The dashed line is the spectrum corresponding to the exponential correlation function.

The data seem to follow the dashed line but fall off rapidly for $k > 1 \quad m^{-1}$. The characteristic vertical scale size is approximately 15 m.

FIGURE 13

According to Chernov (reference 9) the inhomogeneities have been modelled as lenticular cells where the contours in Fig. 13 represent the two-dimensional correlation contours. For acoustic wavelengths smaller than the scale of the inhomogeneities effects are frequency-independent and the ray diffusion equation applies. A plane wave travelling through the inhomogeneous layer becomes corrugated, the variance of the angular distribution increasing linearly with distance.

FIGURE 14

Figure 14 shows a plane wave travelling through the randomly inhomogeneous medium before suffering total internal reflection in the thermocline. Since the horizontal structure was not known, the horizontal and vertical correlation lengths have been assumed equal, hence the estimate represents a lower limit. The gain scale refers to the relative levels at various penetration depths into the thermocline. If there is a surface channel as shown by the dashed line, the surface channel in this case would be excited by scattering at a level of 20 dB below the original level.

FIGURE 15

Acoustic measurements at the Maltese front (reference 10) showed that predicted shadow zones were invariably excited by scattered signals. Figure 15 shows propagation loss in the shadow zone at 250 and 8000 Hz. The shadow zone levels are only 10-20 dB low and the frequency independence is obvious.

SOUND CHANNELS

FIGURE 16

Leakage of signal energy out of sound channels by scatter has been observed in a number of cases (references 11-13) as an additional component of attenuation that is independent of frequency.

To see if the scatter loss explanation is plausible a simple sound channel loss formula was developed (Fig. 16). The sound channel loss depends on both the diffusion constant μ^2/a_o and the strength of the sound channel. Since energy is lost only into the bottom, a linear gradient below the sound channel axis is assumed hence the strength depends only on the distance from the axis to the bottom. For the value $\mu^2 = 10^{-7}$, $a_o = 10$ m and $\Delta z = 2000$ m we show good agreement with the larger values of loss observed in deep sound channels. For lenticular scatterers the results should be multiplied by the ratio of horizontal to vertical scale size.

FIGURE 17

When both scale sizes are 10 m or larger, scatter loss in sound channels should be quite independent of frequency at least above 10 Hz or so. For smaller scale sizes the acoustic wavelength may be sufficiently large for frequency dependence to be observable. Figure 17 shows the Baffin Bay experimental results together with predicted absorption plus scatter loss (reference 14). A rapid falloff below 200 Hz was observed which may be the Rayleigh regime where the scatter cross section varies as k^4. In this case the scale size of the scatterers must be only about 3 m. The rapid transition between regimes also suggests spherical scatterers.

FIGURE 18

In the KIWI experiment (reference 15), shots were dropped by aircraft over a 10,000 km track and signals were received at both ends. The regions B, DA and C exhibit somewhat different sound speed profiles. Other significant features are the polar front and the Louisville ridge.

FIGURE 19

Figure 19 shows propagation loss minus cylindrical spreading at 125 Hz from observations made simultaneously at opposite ends of the track. At this frequency absorption is negligible. The strong increase in loss in the central region seen in both sets of data is attributed to greater scatter.

SEA MOUNTS AND UPWELLING

Another curious phenomenon is observed near the Louisville ridge. A reduction in signal level is expected but the subsequent

recovery at longer ranges is remarkable. Similar results were found by Northrup (reference 16) in transmission measurements across the Hawaiian arch.

FIGURE 20

Experiments were carried out by DSE (reference 17) to investigate the phenomenon. Figure 20 shows the received levels as a function of distance crossing the ridge. Notice that the level drops off before encountering the ridge, then continues to drop off for another 50 miles and subsequently recovering. Further, the effect appears to be quite independent of frequency, hence diffraction is not the answer. Oceanographic measurements show strong upwelling in the vicinity of the ridge and refraction may account for these results.

EDDIES

FIGURE 21

Eddies have recently been found to be more ubiquitous than previously thought and are part of the acoustic prediction problem. They should be acoustically interesting because they can involve all of the phenomenon discussed. Moreover, their rotational speeds can be large (3 kts) over rather large distances (100 km) magnifying the effects. Figure 21 shows the 240 m isotherms of an eddy in the process of formation off the coast of Australia (reference 18). The 18° C core persists to depths in excess of 400 m.

FIGURE 22

Figure 22 shows the propagation loss at 125 Hz for 200 m shots and receivers at 40 and 240 m. The smooth curve is the

mean predicted loss with no eddy present, showing the shadow zone and one convergence. If eddy effects are included in a range dependent ray program the results are much better, but a detailed knowledge of the eddy structure is required.

CONCLUSION

I have attempted to review a few of the recent attempts to bring oceanography to bear on underwater acoustic problems. John Bethell (reference 19) in his recent survey of the literature comments in his conclusions, "The history presents a sad lack of communications between acousticians and oceanographers." The recent progress has been a little more encouraging.

REFERENCES

(1) T. B. Sanford, "Observations of Strong Current Shears in the Deep Ocean and Some Implications on Sound Rays," JASA 56, 1118-1121 (1974).

(2) W. Krauss, P. Koske, J. Kielmann, "Observations on Scattering Layers and Thermocline in the Baltic Sea," Kieler Meereskunde, 85-89 (1974).

(3) R. P. Porter, R. C. Spindel, R. J. Jaffee, "Acoustic-Internal Wave Interactions at Long Ranges in the Ocean," JASA 56, 1426-1436 (1974).

(4) G. E. Stanford, "Low Frequency Fluctuations of a CW Signal in the Ocean," JASA 55, 968-977 (1974).

(5) J. C. Beckerle, H. W. Brock, E. O. LaCasce, "Study of Acoustical Fluctuations and Ocean Movements over One Deep-Ocean Skip Distance," JASA 57, 832-838 (1975).

(6) D. E. Weston, H. W. Andrews, "Acoustical Fluctuations Due to Shallow-Water Internal Waves," J. Sound and Vib. 31 (3), 357-367 (1973).

(7) M. G. Briscoe, O. M. Johannessen, S. Vincenzi, "The Maltese Oceanic Front: A Surface Description by Ship and Aircraft," Deep Sea Research, Vol. 21, p. 247-262 (1974).

(8) R. H. Mellen, "Ray Diffusion in an Ocean-Front Region," SACLANTCEN Memo SM22, 15 Sep 1973.

(9) L. A. Chernov, "Wave Propagation in a Random Medium," McGraw Hill, NY (1960).

(10) SACLANTCEN Unpublished Data.

(11) R. J. Urick, "Low Frequency Sound Attenuation in the Deep Ocean," JASA 35, 1413-1422 (1963).

(12) A. C. Kibblewhite, R. N. Denham, "Low Frequency Sound Absorption in the South Pacific Ocean," JASA 45, 810-815 (1971).

(13) R. H. Mellen and D. G. Browning, "Attenuation in Randomly Inhomogeneous Sound Channels," JASA 56, 80-82 (1974).

(14) R. H. Mellen and D. G. Browning, "Low-Frequency Sound Attenuation in Baffin Bay," JASA 57, 1201-1202 (1975).

(15) D. G. Browning, W. R. Schumacher, R. W. Bannister, R. N. Denham, "Project KIWI ONE: Low-Frequency Sound Attenuation Measurements in the South Pacific Ocean," NUSC Technical Report 4949 (1975).

(16) J. Northrup, "Underwater Sound Propagation Across the Hawaiian Arch," JASA 48, 417 (1970).

(17) R. W. Bannister, Defence Scientific Establishment Report in Preparation.

(18) P. Scully-Power, C. Wilson, P. Nysen, J. Andrews, R. Bannister, D. Browning, "Project ANZUS EDDY: Measurement of a Warm-Core Ocean Eddy," Preliminary Report Royal Australian Navy Research Laboratory, 1 April 1975.

(19) J. P. Bethell, "The Fine Structure of the Ocean: A Review," SACLANTCEN Technical Memorandum No. 184, 15 Dec 1972.

* MICROSTRUCTURE
* TURBULENCE
* LAYERS
* INTERNAL WAVES
* FRONTS
* EDDIES
* WATER MASSES
* GYRES

FIG. 1
OCEAN INHOMOGENEITIES

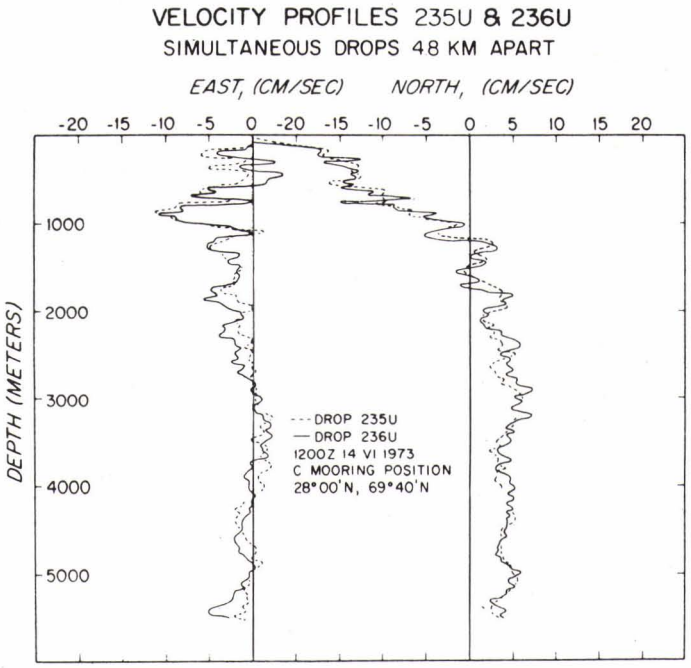

FIG. 2
MICROCURRENTS IN THE SARGASSO SEA
(Reference 1)

Pair of velocity profiles taken at separate locations but simultaneously in time.

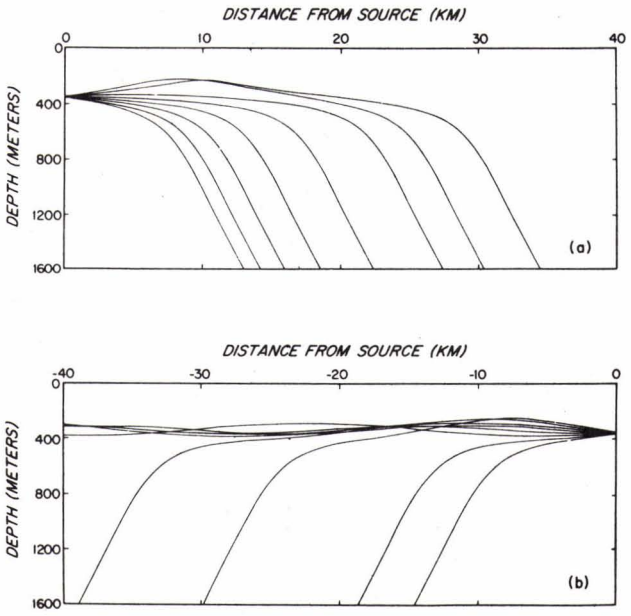

FIG. 3
NONRECIPROCAL RAYS IN CURRENT SHEAR
(Reference 1)

Ray paths for (a) propagation in direction of current and (b) propagation against current.

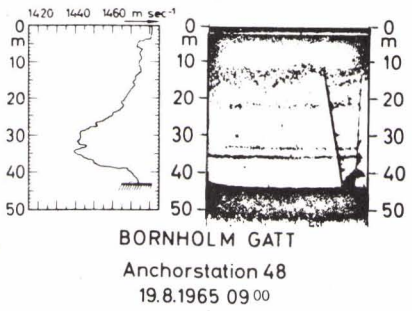

FIG. 4
BACKSCATTER FROM A TURBULENT BOUNDARY (Reference 2)

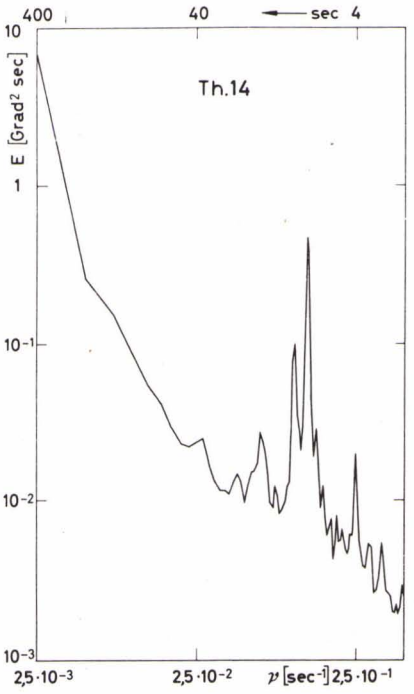

FIG. 5
TEMPERATURE SPECTRUM OF TURBULENT BOUNDARY WITH PEAK NEAR THE BUOYANCY FREQUENCY
(Reference 2)

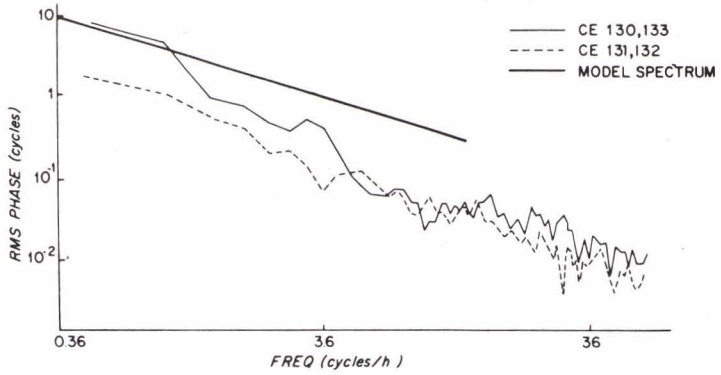

FIG. 6
ACOUSTIC PHASE FLUCTUATION SHOWING ACTIVITY ABOVE THE BUOYANCY FREQUENCY
(Reference 3)

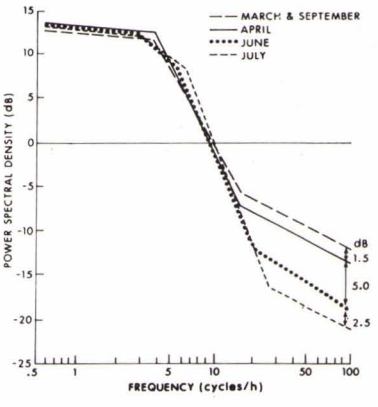

FIG. 7
AMPLITUDE FLUCTUATION SPECTRUM OF SIGNALS BETWEEN BERMUDA AND ELEUTHERA
(Reference 4)

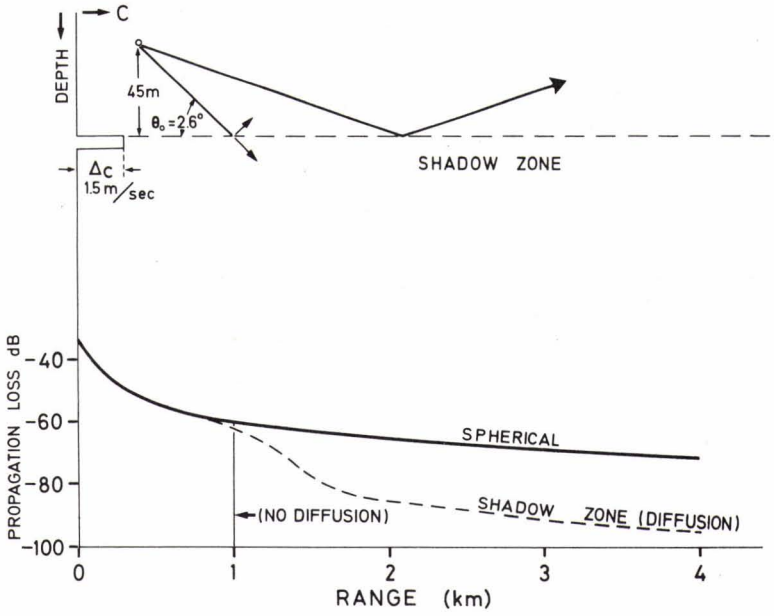

FIG. 8
SCATTERING LOSS THROUGH A TURBULENT LAYER

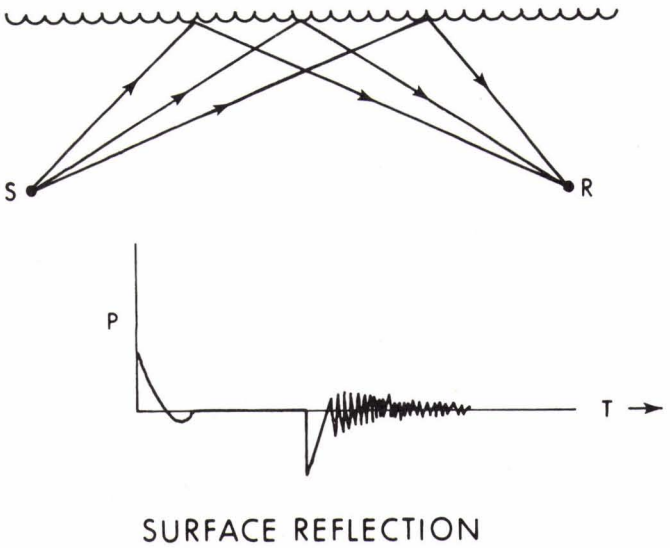

FIG. 9
SCHEMATIC OF PULSE REFLECTED FROM A ROUGH SURFACE

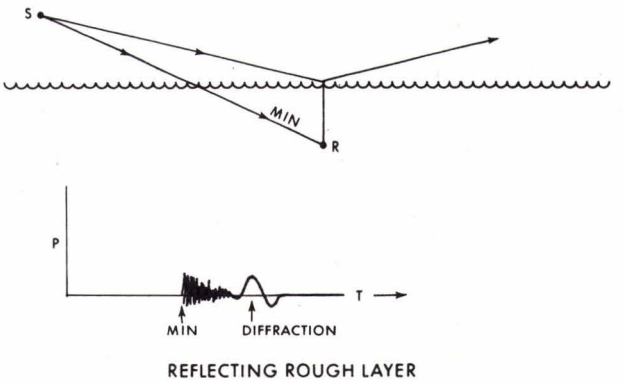

FIG. 10
SCHEMATIC OF PULSE TRANSMITTED THROUGH A ROUGH LAYER

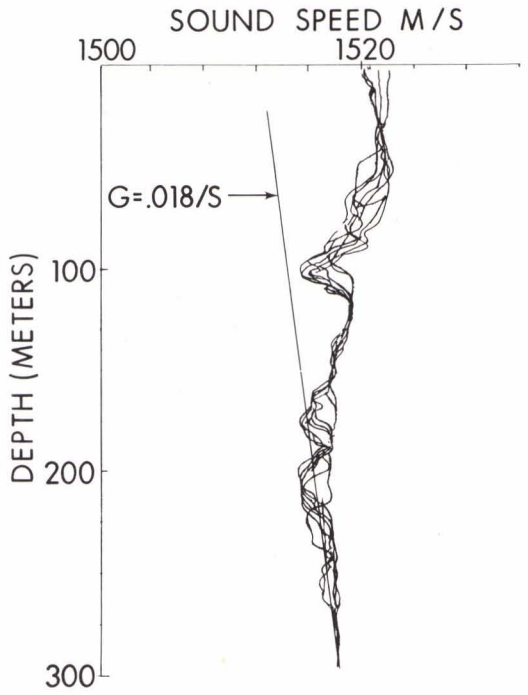

FIG. 11
SOUND SPEED PROFILES OF THE MALTESE FRONT
(Reference 8)

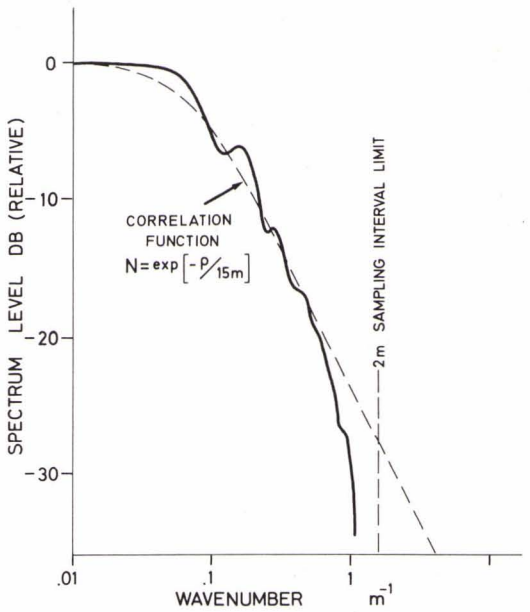

FIG. 12
WAVE NUMBER SPECTRUM OF RANDOM SSP FLUCTUATIONS OF THE MALTESE FRONT
(Reference 8)

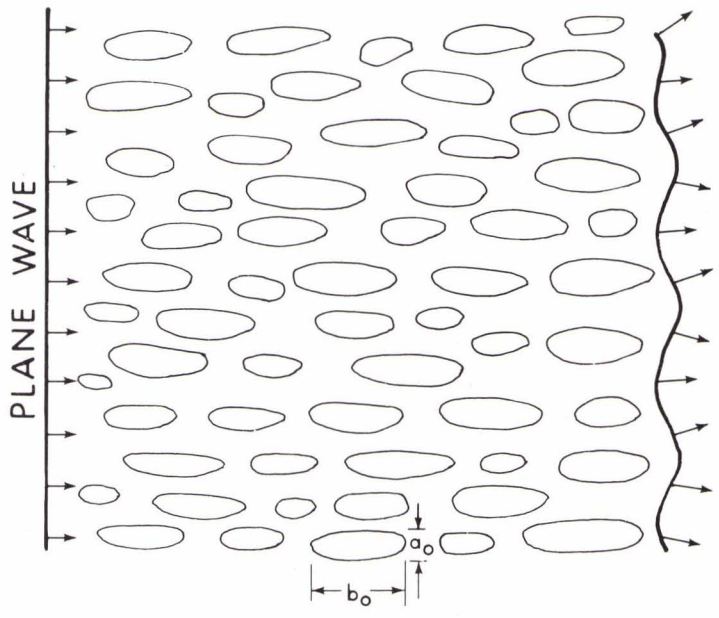

FIG. 13
PLANE WAVE TRAVELING IN A RANDOMLY INHOMOGENEOUS MEDIUM

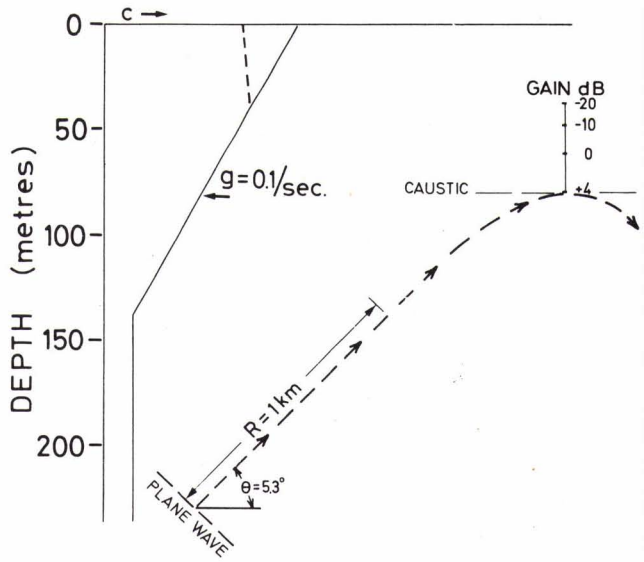

FIG. 14
PLANE WAVE TOTALLY REFLECTED IN A RANDOMLY INHOMOGENEOUS THERMOCLINE SHOWING RELATIVE LEVELS ABOVE THE CAUSTIC

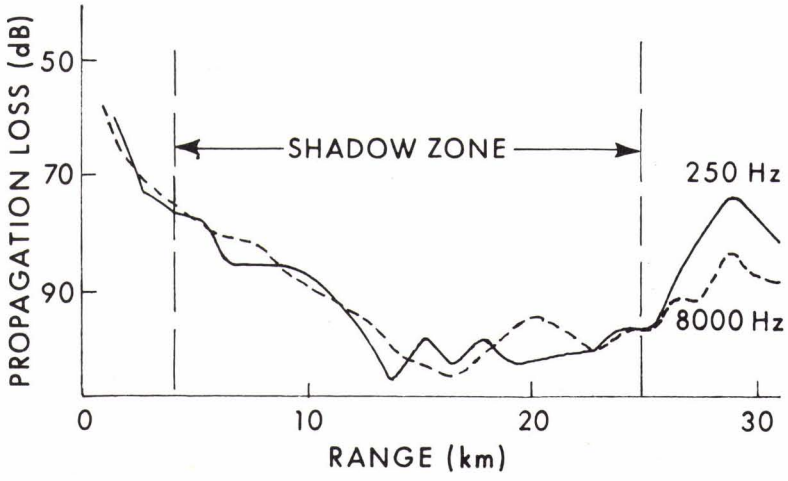

FIG. 15
MEASURED PROPAGATION LOSS AT THE MALTESE FRONT SHOWING FREQUENCY INDEPENDENCE OF SCATTER INTO THE SHADOW ZONE (Reference 10)

SCATTERING FORMULA

$$\alpha = 8 \times 10^{8} \frac{\mu^2}{a_o \Delta Z} \quad \text{dB/km}$$

TYPICAL VALUES

$\mu^2 = 10^{-7}$ $\quad \Delta Z = 2\,(\text{km})$

$a_o = 10\,(\text{m})$ $\quad \alpha = .004$ dB/km

FIG. 16
SOUND CHANNEL LOSS FORMULA
(Reference 13)

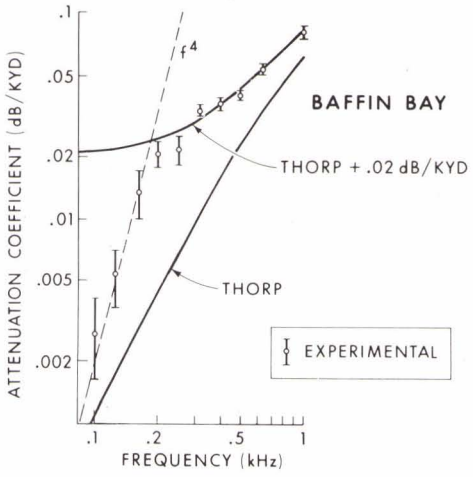

FIG. 17
BAFFIN BAY ATTENUATION VS. FREQUENCY SHOWING RAYLEIGH REGION BELOW 200 Hz
(Reference 14)

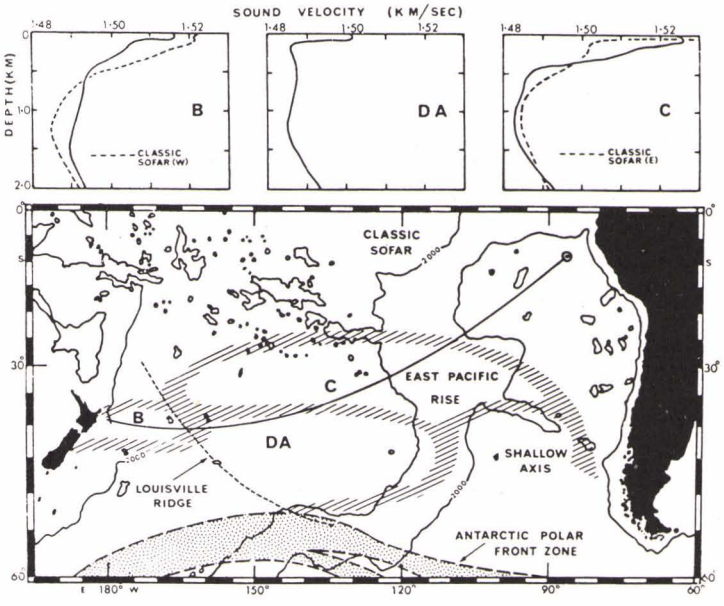

FIG. 18
THE KIWI EXPERIMENT (Reference 15)

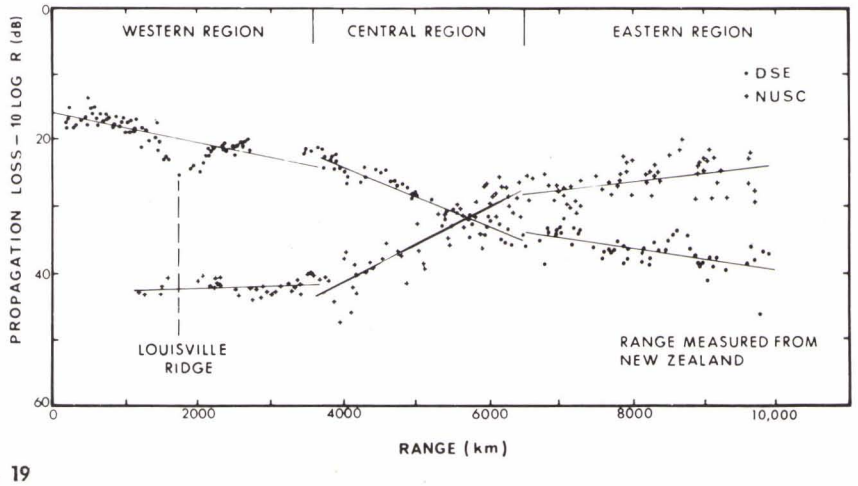

FIG. 19
KIWI PROPAGATION LOSS MINUS SPHERICAL SPREADING AT 125 Hz MEASURED AT BOTH ENDS OF THE TRACK (Reference 15)

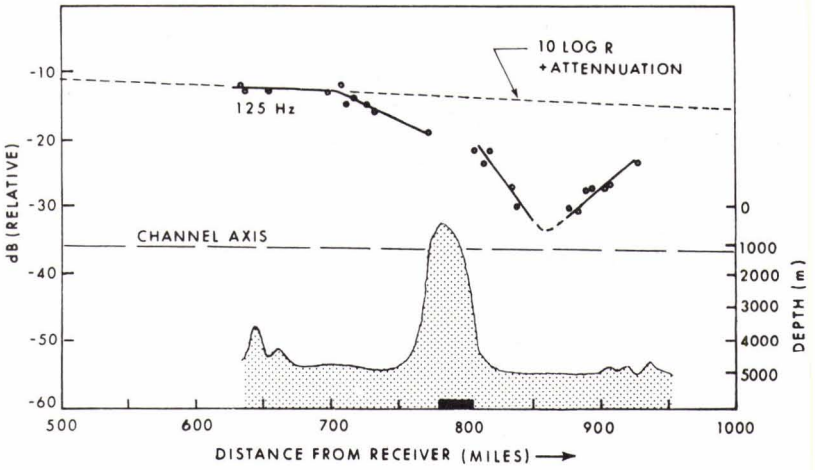

FIG. 20
PROPAGATION LOSS ACROSS THE LOUISVILLE RIDGE
(Reference 17)

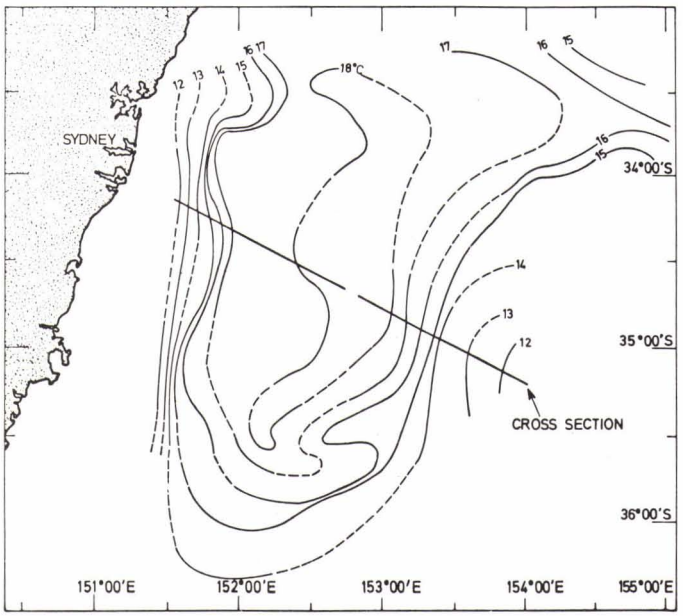

FIG. 21
AUSTRALIAN EDDY – 240 m ISOTHERMS
(Reference 18)

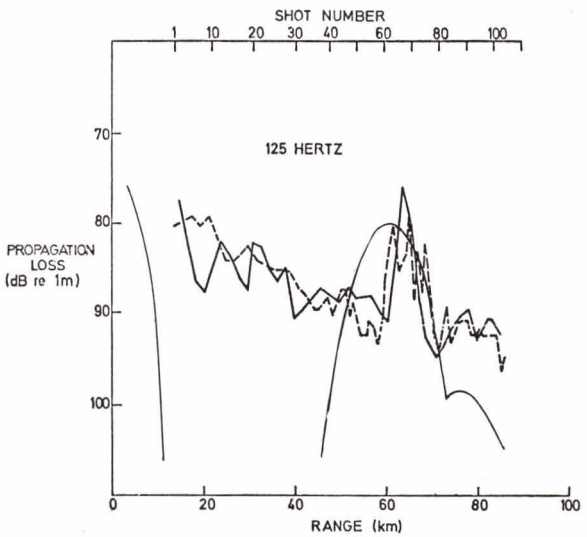

FIG. 22
AUSTRALIAN EDDY PROPAGATION LOSS (Edge to Center) FOR RECEIVER AT 200 m AND SHOTS AT 40 m (Solid Line) AND 240 m (Dashed Line). SMOOTH CURVE IS AVERAGE PROPAGATION LOSS WHEN NO EDDY IS PRESENT (Reference 18)